Sensors and Materials, Vol. 35, No. 2 (2023) 459–466
MYU Tokyo

S & M 3182

Radiation-induced Luminescence Properties of Tm-doped $Bi_4Ge_3O_{12}$ Single Crystals

Kai Okazaki,* Daisuke Nakauchi, Hiroyuki Fukushima, Takumi Kato, Noriaki Kawaguchi, and Takayuki Yanagida

Division of Materials Science, Nara Institute of Science and Technology (NAIST), 8916-5 Takayama-Cho, Ikoma, Nara 630-0192, Japan

(Received October 28, 2022; accepted January 5, 2023)

Keywords: scintillator, near-IR, floating zone method, dose rate response, scintillation detector

We grew 0.1, 0.5, and 1% Tm-doped $Bi_4Ge_3O_{12}$ single crystals by the floating zone method. Their photoluminescence and scintillation properties were investigated in the range from visible to near-IR. Luminescence spectra and decay times consistent with the transitions of Tm^{3+} were confirmed. X-ray-irradiated dose rate response properties were evaluated using the prepared samples and an InGaAs photodiode. The 1% Tm-doped sample showed the widest dynamic range (0.03–60 Gy/h) among the prepared samples.

1. Introduction

Scintillators are materials that instantaneously convert X- and γ-rays into numerous low-energy photons after absorbing the energy of the X- and γ-rays. Their application fields include medicine,[1] security,[2] oil exploration,[3] and high-energy physics.[4] Because the physical and chemical properties of each scintillator are different, the most suitable one is selected on the basis of the requirements of the application. Various material forms have been used as scintillators, such as crystals,[5–9] ceramics,[10,11] glasses,[12–14] and liquids.[15–18] To date, scintillators emitting UV–visible photons have been mainly studied because they have been used in combination with photodetectors having wavelength sensitivity in the UV–visible ranges[19] such as photomultiplier tubes (PMTs) and Si photodiodes (PDs). With the development of photodetectors having wavelength sensitivity in the near-IR (NIR) range, NIR scintillators have recently attracted interest.

NIR scintillators are expected to be used for high-dose field monitoring, such as in real-time *in vivo* dose monitoring during radiotherapy.[20] In the therapy, scintillators are inserted near the target cancers, and NIR photons can be read out by a detector outside of the patient's body. In addition, NIR scintillators could be used for monitoring nuclear reactors.[21] For such an application, a remote monitoring system with quartz optical fibers has been proposed.[22] NIR photons have low transmission loss in the optical fiber compared with visible photons;[23] thus, dose measurement in a wide dynamic range can be achieved. The interaction cross section for

*Corresponding author: e-mail: okazaki.kai.of0@ms.naist.jp
https://doi.org/10.18494/SAM4144

ISSN 0914-4935
https://myukk.org/

X- and γ-rays is proportional to ρZ_{eff}^4,[24] where ρ and Z_{eff} are, respectively, the density and effective atomic number. NIR scintillators with a high ρ and large Z_{eff} have been developed[25,26] as well as UV–visible scintillators.[27,28] Hence, $Bi_4Ge_3O_{12}$ (BGO) having a high ρ (7.13 g/cm^3) and large Z_{eff} (75) is a candidate host material for NIR scintillators. Tm has been used as an NIR luminescence center in laser fields for medical[29] and welding[30] applications. Additionally, the NIR scintillation of Tm has been reported.[31–33] For high-dose field monitoring near and inside a nuclear reactor, NIR scintillators need to detect a dose rate of 0.1 mGy/h.[21] In this study, we fabricated BGO single crystals with different concentrations of Tm, the photoluminescence (PL) and scintillation properties of which were evaluated.

2. Materials and Methods

BGO single crystals doped with 0.1, 0.5, and 1 at% Tm were prepared by the floating zone (FZ) method. Bi_2O_3 (Mitsuwa Chemicals, 99.99%), GeO_2 (Furuuchi Chemical, 99.999%), and Tm_2O_3 (Furuuchi Chemical, 99.9%) were first mixed as starting materials. Then, the powders were molded into rod shapes and sintered at 800 ℃ for 8 h to prepare polycrystalline rods. Crystal growth was conducted using an FZ furnace (Canon Machinery, FZD0192). To confirm the crystal phase of the obtained crystals, the powder X-ray diffraction (XRD) pattern was measured with a diffractometer (Rigaku, MiniFlex600). PL properties were investigated using Quantaurus-QY Plus and Quantaurus-τ systems (Hamamatsu Photonics, C13534 and C11367). The X-ray-induced scintillation properties were measured using our original setups.[2,34–36]

3. Results and Discussion

Figure 1 shows the appearance of the samples. After the single-crystal growth, we obtained rod-shaped transparent samples with dimensions of ~20 mm × 5 mm ϕ. The obtained rods were cut and polished for PL and scintillation measurements. Figure 2 shows the XRD patterns of the samples, where some parts of the rod crystals were crushed into powder for the measurement. The confirmed patterns agreed with the reference pattern of BGO from the Crystallography Open Database (COD: 1007142), and no other phases were observed; thus, the samples have a single phase of BGO with cubic symmetry and a space group of *I*-43*d*.

Figure 3 shows the PL excitation and emission spectra of the 0.1% Tm-doped sample. Because all the samples produced spectra with similar shapes, the spectra of the 0.1% Tm-doped sample were exhibited as representatives. Under excitation at 280 nm, a broad emission band due to the $^3P_1$–$^1S_0$ transition of Bi^{3+} was observed at 400–750 nm.[37] Additionally, sharp emission peaks were confirmed at 480 and 800 nm. They were respectively considered to be derived from the $^1G_4$–$^3H_6$ and $^3H_4$–$^3H_6$ transitions of Tm^{3+}[37,38] through energy transfer from Bi^{3+} to Tm^{3+} since the excitation wavelength (280 nm) corresponded to the $^1S_0$–$^3P_1$ transition of Bi^{3+}.[39] Emission at 800 nm due to Tm^{3+} was observed under excitation at 680 nm. The quantum yields (*QY*s) of 0.1, 0.5, and 1% Tm-doped BGO monitored at 750–1700 nm under excitation at 650 nm were 56.7, 23.8, and 19.1%, respectively. The 0.1% Tm-doped BGO showed a relatively high *QY* compared with BGO doped with other rare earths, because the *QY*s of Nd-, Er-, Pr-, and Yb-doped BGO

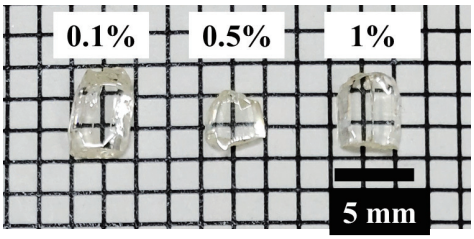

Fig. 1. (Color online) Photograph of prepared Tm-doped BGO.

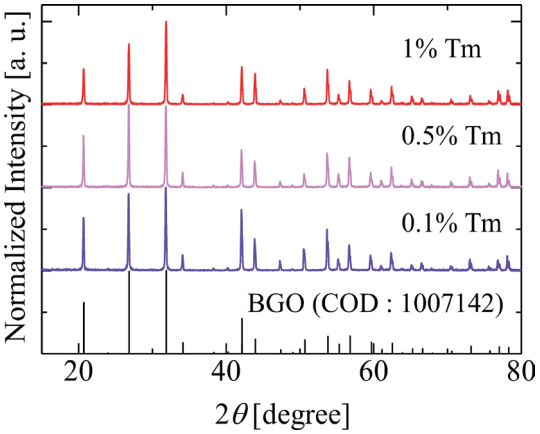

Fig. 2. (Color online) XRD patterns of Tm-doped BGO.

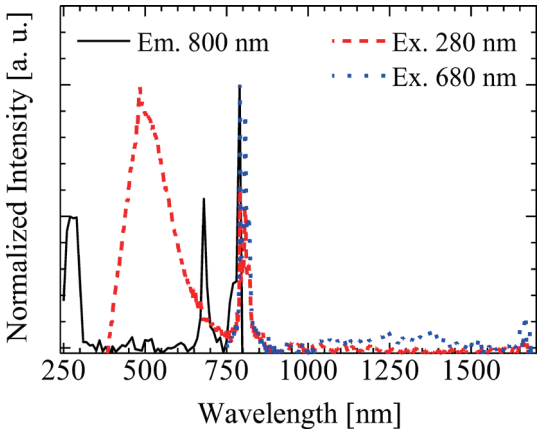

Fig. 3. (Color online) PL excitation (solid line) and emission (dashed line) spectra of 0.1% Tm-doped BGO.

samples with the optimum doping concentration in the NIR range were respectively reported to be 43, 86, 35, and 26%.[39–42] The PL decay curves of the samples are shown in Fig. 4. The excitation and monitored wavelengths were 600–690 and 810 nm, respectively. The decay curves were approximated by a single exponential function. The decay time constants (~400 μs) were typical values for the $^3H_4$–$^3H_6$ transition of Tm^{3+} because almost the same decay times were confirmed for other Tm-doped phosphors.[33,43] The decay time constants decreased as the Tm concentration increased. On the basis of the tendency of the *QY*, this is considered to have been caused by the concentration quenching of Tm.

Figure 5 shows the X-ray-induced scintillation spectra of the samples. Sharp emission peaks were observed at 480, 650, 800, 1200, and 1450 nm. They were attributed to the 4f–4f transition of Tm^{3+} because similar peaks were observed for other Tm-doped materials.[33,44] The relative emission intensities of Tm^{3+} at 480 and 650 nm increased as the Tm concentration increased. The emission at 1600 nm was considered to have originated from the $^3F_4$–$^3H_6$ transition.[45] Broad emission bands due to the $^3P_1$–$^1S_0$ transition of Bi^{3+} were additionally confirmed at 400–700 nm.[46]

The X-ray-induced scintillation decay curves monitored at 160–650 nm and 380–900 nm are shown in Fig. 6. The decay curves monitored at 160–650 nm were composed of a sum of three

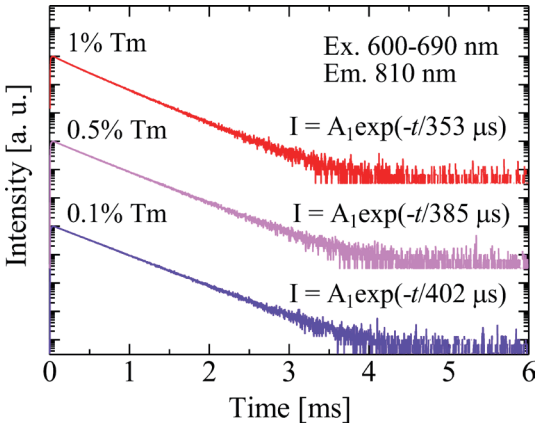

Fig. 4. (Color online) PL decay curves of Tm-doped BGO monitored at 810 nm under excitation at 600–690 nm.

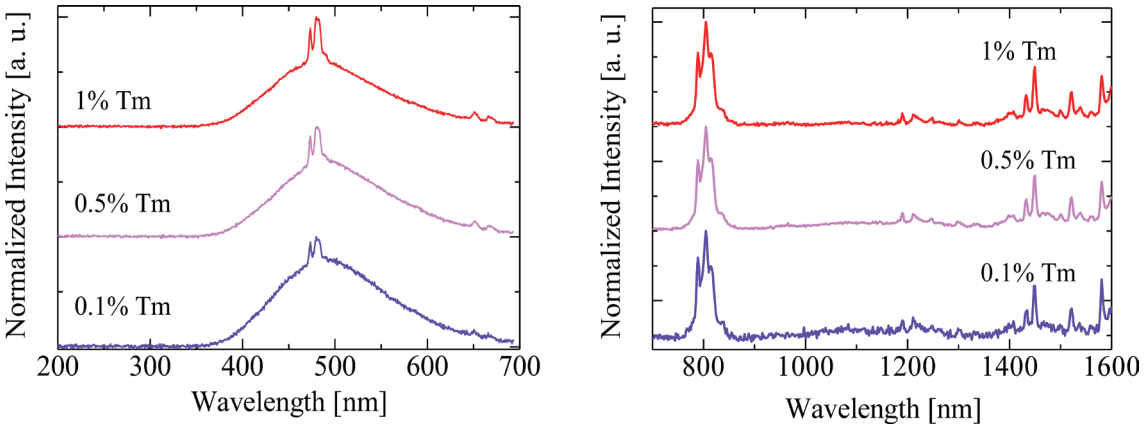

Fig. 5. (Color online) X-ray-induced scintillation spectra of Tm-doped BGO at (a) 200–700 nm and (b) 700–1600 nm.

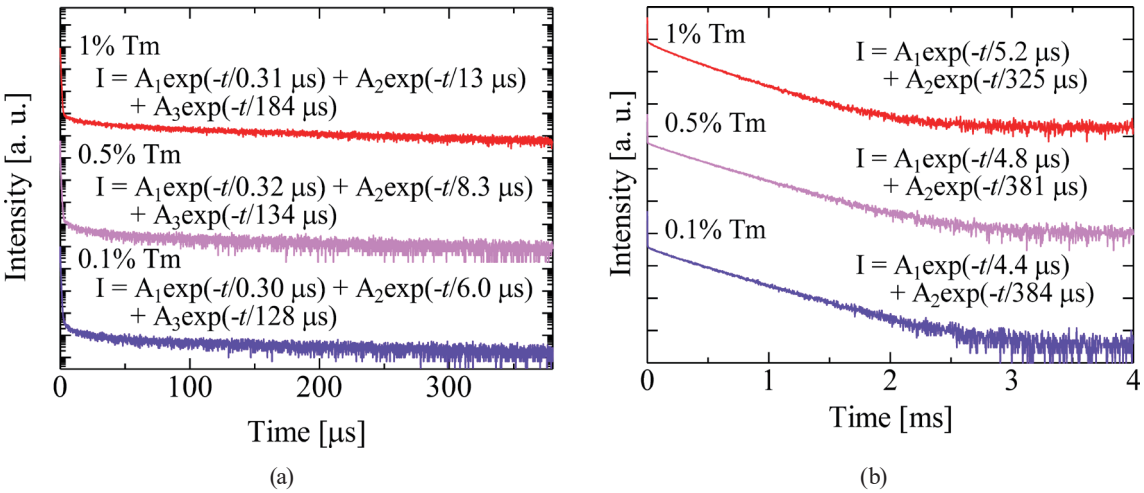

Fig. 6. (Color online) X-ray-induced scintillation decay curves of Tm-doped BGO monitored at (a) 160–650 nm and (b) 380–900 nm.

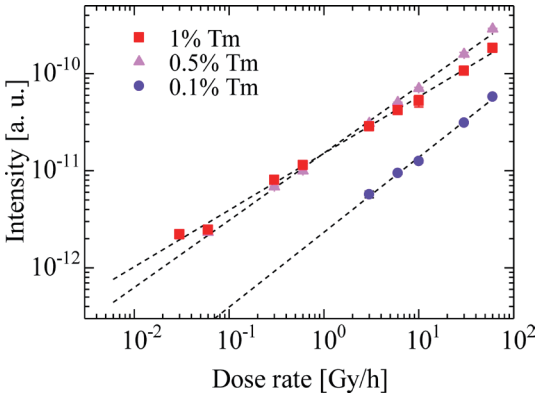

Fig. 7. (Color online) Relationship between emission intensity of Tm-doped BGO and X-ray exposure dose rate.

exponential functions. The fastest component (~300 ns) was derived from the transitions of Bi^{3+}.[47] The other two components with decay times of ~6–13 μs and ~130–180 μs originated from the 4f–4f transitions of Tm^{3+} because the obtained decay times were close to those of Tm-doped $Lu_2Si_2O_7$.[48] The decay curves monitored at 380–900 nm were in good agreement with the sum of two exponential functions. Both the fast (~5 μs) and slow (~320–380 μs) components originated from the 4f–4f transitions of Tm^{3+} because they had almost the same values as those of Tm-doped $GdAlO_3$ monitored in the same ranges.[49] A decay time of ns order is preferred for photon counting; however, a decay time of 100 μs to ms order is acceptable for an integrated-type measurement such as dose field monitoring.[2]

Figure 7 shows the relationship between the X-ray-irradiated dose rate (horizontal axis) and the NIR scintillation intensity (vertical axis). The intensity is presented as the average current during X-ray irradiation minus the average background current before and during X-ray irradiation. The dashed lines indicate an approximation to a power function. The lowest detection limits for which the linearity of the 0.1, 0.5, and 1% Tm-doped samples was retained were respectively 3, 0.06, and 0.03 Gy/h when the error bar of the intensity was defined as three standard deviations following a previous study.[41] The lowest limit was superior to that of Pr-doped Gd_2O_2S measured with a Si charge-coupled device.[21] However, the limit was inferior to that measured using BGO doped with other rare earths with an InGaAs PD.[39–42] The main emission of Tm^{3+} appeared at 800 nm as shown in Fig. 5. The quantum efficiency of InGaAs at 800 nm is ~16%, whereas that at 1000–1600 nm is ~70–88%. Hence, the emission wavelength of Tm^{3+} is unsuitable for the sensitivity of an InGaAs PD, and it can contribute to narrow dynamic ranges.

4. Conclusions

Tm-doped BGO single crystals with various concentrations (0.1, 0.5, and 1%) were successfully synthesized by the FZ method. Emission peaks due to 4f–4f transitions of Tm^{3+} were observed in the NIR region. The relationship between the X-ray-irradiated dose rate and the intensity in the NIR range was evaluated using an InGaAs PD. Among the present samples,

the lowest detection limit was 0.03 Gy/h for the 1% Tm-doped BGO, which is inferior to the values for BGO doped with other rare earths. Although the Tm-doped BGO exhibited the highest peak intensity at 800 nm, its emission wavelength is not suitable for an InGaAs PD with spectral sensitivity. Since Tm-doped BGO has emission bands at ~800 nm and ~1400–1600 nm, upon its combination with a Si PD, its detection limit will be improved owing to the quantum efficiency of the Si PD at 800 nm (~85%).

Acknowledgments

This work was supported by Grants-in-Aid for Scientific Research A (22H00309), Scientific Research B (21H03733, 21H03736, and 22H03872), and Exploratory Research (22K18997) from the Japan Society for the Promotion of Science. JST A-STEP, Foundation from Cooperative Research Project of the Research Center for Biomedical Engineering, Nippon Sheet Glass Foundation, Terumo Life Science Foundation, Iwatani Naoji Foundation, and Konica Minolta Science and Technology Foundation are also acknowledged.

References

1 P. Lecoq: Nucl. Instrum. Methods Phys. Res., Sect. A **809** (2016) 130. https://doi.org/10.1016/j.nima.2015.08.041
2 T. Yanagida, Y. Fujimoto, T. Ito, K. Uchiyama, and K. Mori: Appl. Phys. Express **7** (2014) 062401. https://doi.org/10.7567/APEX.7.062401
3 C. L. Melcher, J. S. Schweitzer, R. A. Manente, and C. A. Peterson: J. Cryst. Growth **109** (1991) 37. https://doi.org/10.1016/0022-0248(91)90155-X
4 R. Mao, L. Zhang, and R.-Y. Zhu: IEEE Trans. Nucl. Sci. **55** (2008) 2425. https://doi.org/10.1109/TNS.2008.2000776
5 D. Nakauchi, Y. Fujimoto, T. Kato, N. Kawaguchi, and T. Yanagida: Crystals **12** (2022) 517. https://doi.org/10.3390/cryst12040517
6 D. Nakauchi, T. Kato, N. Kawaguchi, and T. Yanagida: Sens. Mater. **33** (2021) 2203. https://doi.org/10.18494/SAM.2021.3323
7 K. Takagi and T. Fukazawa: Appl. Phys. Lett. **42** (1983) 43. https://doi.org/10.1063/1.93760
8 K. Okazaki, D. Onoda, D. Nakauchi, N. Kawano, H. Fukushima, T. Kato, N. Kawaguchi, and T. Yanagida: Sens. Mater. **34** (2022) 575. https://doi.org/10.18494/SAM3678
9 D. Nakauchi, H. Fukushima, T. Kato, N. Kawaguchi, and T. Yanagida: Sens. Mater. **34** (2022) 611. https://doi.org/10.18494/SAM3696
10 T. Kunikata, T. Kato, D. Shiratori, D. Nakauchi, N. Kawaguchi, and T. Yanagida: Sens. Mater. **34** (2022) 661. https://doi.org/10.18494/SAM3683
11 Y. Lan, B. Mei, W. Li, F. Xiong, and J. Song: J. Lumin. **208** (2019) 183. https://doi.org/10.1016/j.jlumin.2018.12.047
12 R. Nakamori, N. Kawano, A. Takaku, D. Nakauchi, H. Kimura, M. Akatsuka, K. Shinozaki, and T. Yanagida: Mater. Res. Bull. **145** (2022) 111547. https://doi.org/10.1016/j.materresbull.2021.111547
13 L. M. Bollinger, G. E. Thomas, and R. J. Ginther: Nucl. Instrum. Methods **17** (1962) 97. https://doi.org/10.1016/0029-554X(62)90178-7
14 G. Ito, H. Kimura, D. Shiratori, D. Nakauchi, T. Kato, N. Kawaguchi, and T. Yanagida: Sens. Mater. **34** (2022) 685. https://doi.org/10.18494/SAM3681
15 G. A. Bray: Anal. Biochem. **1** (1960) 279. https://doi.org/10.1016/0003-2697(60)90025-7
16 T. Doke, A. Hitachi, J. Kikuchi, K. Masuda, H. Okada, and E. Shibamura: Jpn. J. Appl. Phys. **41** (2002) 1538. https://doi.org/10.1143/JJAP.41.1538
17 A. Watanabe, A. Magi, M. Koshimizu, A. Sato, Y. Fujimoto, and K. Asai: Sens. Mater. **33** (2021) 2251. https://doi.org/10.18494/SAM.2021.3411
18 M. Yeh, S. Hans, W. Beriguete, R. Rosero, L. Hu, R. L. Hahn, M. V. Diwan, D. E. Jaffe, S. H. Kettell, and L. Littenberg: Nucl. Instrum. Methods Phys. Res., Sect. A **660** (2011) 51. https://doi.org/10.1016/j.nima.2011.08.040

19 H. Kimura, T. Kato, D. Nakauchi, N. Kawaguchi, and T. Yanagida: Sens. Mater. **33** (2021) 2187. https://doi.org/10.18494/SAM.2021.3322
20 L. Archambault, T. M. Briere, F. Pönisch, L. Beaulieu, D. A. Kuban, A. Lee, and S. Beddar: Int. J. Radiat. Oncol. **78** (2010) 280. https://doi.org/10.1016/j.ijrobp.2009.11.025
21 E. Takada, Y. Hosono, T. Kakuta, M. Yamazaki, H. Takahashi, and M. Nakazawa: IEEE Trans. Nucl. Sci. **45** (1998) 556. https://doi.org/10.1109/23.682447
22 A. N. Gurzhiev, L. K. Turchanovich, V. G. Vasil'chenko, V. A. Bogatyrjov, and V. M. Mashinsky: Nucl. Instrum. Methods Phys. Res., Sect. A **391** (1997) 417. https://doi.org/10.1016/S0168-9002(97)00395-1
23 H. Sakr, Y. Chen, G. T. Jasion, T. D. Bradley, J. R. Hayes, H. C. H. Mulvad, I. A. Davidson, E. Numkam Fokoua, and F. Poletti Nat. Commun. **11** (2020) 6030. https://doi.org/10.1038/s41467-020-19910-7
24 C. W. E. van Eijk: Nucl. Instrum. Methods Phys. Res., Sect. A **509** (2003) 17. https://doi.org/10.1016/S0168-9002(03)01542-0
25 M. Akatsuka, D. Nakauchi, T. Kato, N. Kawaguchi, and T. Yanagida: Jpn. J. Appl. Phys. **61** (2022) SB1025. https://doi.org/10.35848/1347-4065/ac2627
26 M. Akatsuka, D. Nakauchi, T. Kato, K. Noriaki, and Y. Takayuki: Sens. Mater. **34** (2022) 619. https://doi.org/10.18494/SAM3692
27 M. Moszynski, M. Balcerzyk, W. Czarnacki, M. Kapusta, W. Klamra, P. Schotanus, A. Syntfeld, and M. Szawlowski: 2002 IEEE Nucl. Sci. Symp. Conf. Rec. (IEEE, 2002) 346. https://doi.org/10.1109/NSSMIC.2002.1239330
28 G. Patton, F. Moretti, A. Belsky, K. Al Saghir, S. Chenu, G. Matzen, M. Allix, and C. Dujardin: Phys. Chem. Chem. Phys. **16** (2014) 24824. https://doi.org/10.1039/C4CP04064C
29 T. Yokozawa and H. Hara: Appl. Opt. **35** (1996) 1424. https://doi.org/10.1364/AO.35.001424
30 I. Mingareev, F. Weirauch, A. Olowinsky, L. Shah, P. Kadwani, and M. Richardson: Opt. Laser Technol. **44** (2012) 2095. https://doi.org/10.1016/j.optlastec.2012.03.020
31 G. Okada, N. Kawaguchi, and T. Yanagida: Sens. Mater. **29** (2017) 1407. https://doi.org/10.18494/SAM.2017.1620
32 M. Akatsuka, D. Nakauchi, T. Kato, N. Kawaguchi, and T. Yanagida: Sens. Mater. **32** (2020) 1373. https://doi.org/10.18494/SAM.2020.2743
33 M. Akatsuka, G. Okada, D. Nakauchi, T. Kato, N. Kawaguchi, and T. Yanagida: J. Lumin. **228** (2020) 117610. https://doi.org/10.1016/j.jlumin.2020.117610
34 H. Fukushima, M. Akatsuka, H. Kimura, D. Onoda, D. Shiratori, D. Nakauchi, T. Kato, N. Kawaguchi, and T. Yanagida: Sens. Mater. **33** (2021) 2235. https://doi.org/10.18494/SAM.2021.3324
35 T. Yanagida, K. Kamada, Y. Fujimoto, H. Yagi, and T. Yanagitani: Opt. Mater. **35** (2013) 2480. https://doi.org/10.1016/j.optmat.2013.07.002
36 M. Akatsuka, H. Kimura, D. Onoda, D. Shiratori, D. Nakauchi, T. Kato, N. Kawaguchi, and T. Yanagida: Sens. Mater. **33** (2021) 2243. https://doi.org/10.18494/SAM.2021.3319
37 R. Kibar, A. Çetin, Y. Tuncer, S. Uysal, P. D. Townsend, A. Canimoglu, T. Karali, and N. Can: Phys. Procedia **2** (2009) 379. https://doi.org/10.1016/j.phpro.2009.07.023
38 Y. T. Arslanlar, Z. Kotan, R. Kibar, A. Canımoğlu, and N. Can: Spectrosc. Lett. **46** (2013) 590. https://doi.org/10.1080/00387010.2013.771370
39 K. Okazaki, H. Fukushima, D. Nakauchi, G. Okada, D. Onoda, T. Kato, N. Kawaguchi, and T. Yanagida: J. Alloys Compd. **903** (2022) 163834. https://doi.org/10.1016/j.jallcom.2022.163834
40 K. Okazaki, D. Onoda, H. Fukushima, D. Nakauchi, T. Kato, N. Kawaguchi, and T. Yanagida: J. Mater. Sci. Mater. Electron. **32** (2021) 21677. https://doi.org/10.1007/s10854-021-06686-9
41 K. Okazaki, H. Fukushima, D. Nakauchi, G. Okada, D. Onoda, T. Kato, N. Kawaguchi, and T. Yanagida: Radiat. Meas. **154** (2022) 106773. https://doi.org/10.1016/j.radmeas.2022.106773
42 K. Okazaki, H. Fukushima, D. Nakauchi, T. Kato, N. Kawaguchi, and T. Yanagida: Jpn. J. Appl. Phys. **61** (2022) 062009. https://doi.org/10.35848/1347-4065/ac6c13
43 R. Arppe, I. Hyppänen, N. Perälä, R. Peltomaa, M. Kaiser, C. Würth, S. Christ, U. Resch-Genger, M. Schäferling, and T. Soukka: Nanoscale **7** (2015) 11746. https://doi.org/10.1039/C5NR02100F
44 Y. Tariwong, P. Q. Vuong, N. T. Luan, S. Saha, H. J. Kim, N. Wantana, N. Chanthima, J. Kaewkhao, and S. Kothan: Radiat. Phys. Chem. **200** (2022) 110347. https://doi.org/10.1016/j.radphyschem.2022.110347
45 J. Ganem and S. R. Bowman: Nanoscale Res. Lett. **8** (2013) 455. https://doi.org/10.1186/1556-276X-8-455
46 S .E. Brunner and D. R. Schaart: Phys. Med. Biol. **62** (2017) 4421. https://doi.org/10.1088/1361-6560/aa6a49
47 J. Gironnet, V .B. Mikhailik, H. Kraus, P. de Marcillac, and N. Coron: Nucl. Instrum. Methods Phys. Res. Res., Sect. A **594** (2008) 358. https://doi.org/10.1016/j.nima.2008.07.008

48 P. Kantuptim, M. Akatsuka, D. Nakauchi, T. Kato, N. Kawaguchi, and T. Yanagida: J. Alloys Compd. **847** (2020) 156542. https://doi.org/10.1016/j.jallcom.2020.156542
49 M. Akatsuka, G. Okada, D. Nakauchi, T. Kato, N. Kawaguchi, and T. Yanagida: J. Lumin. **228** (2020) 117610. https://doi.org/10.1016/j.jlumin.2020.117610